BIOCHEMISTRY
including biophysical chemistry & molecular biology

Article

pubs.acs.org/biochemistry

Structural and Mechanistic Studies of HpxO, a Novel Flavin Adenine Dinucleotide-Dependent Urate Oxidase from *Klebsiella pneumoniae*

Katherine A. Hicks,[†] Seán E. O'Leary,[†,‡] Tadhg P. Begley,*[,‡] and Steven E. Ealick*[,†]

[†]Department of Chemistry and Chemical Biology, Cornell University, Ithaca, New York 14853, United States

[‡]Department of Chemistry, Texas A&M University, College Station, Texas 77842, United States

Supporting Information

ABSTRACT: HpxO is a flavin-dependent urate oxidase that catalyzes the hydroxylation of uric acid to 5-hydroxyisourate and functions in a novel pathway for purine catabolism found in *Klebsiella pneumoniae*. We have determined the structures of HpxO with and without uric acid at 2.0 and 2.2 Å, respectively. We have also determined the structure of the R204Q variant at 2.0 Å resolution in the absence of uric acid. The variant structure is very similar to that of wild-type HpxO except for the conformation of Arg103, which interacts with FAD in the variant but not in the wild-type structure. Interestingly, the R204Q variant results in the uncoupling of nicotinamide adenine dinucleotide oxidation from uric acid hydroxylation. This suggests that Arg204 facilitates the deprotonation of uric acid, activating it for the oxygen transfer. On the basis of these data, a mechanism for this reaction consisting of a nucleophilic attack of the urate anion on the flavin hydroperoxide resulting in the formation of 5-hydroxyisourate is proposed.

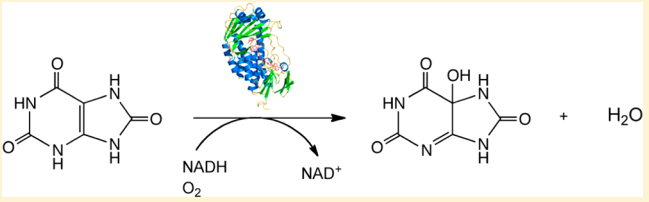

The ubiquitous pathogen *Klebsiella pneumoniae* is a Gram-negative bacterium often responsible for pneumonia, wound infection, and urinary tract infections in hospital and health care settings.[1] *K. pneumoniae* can also be a community-acquired pathogen causing liver abscess and meningitis.[2] This bacterium has developed resistance to a wide range of antibiotics, including carbapenems, which are used as a last line of defense against Gram-negative infections. Within the past decade, carbapenem-resistant *K. pneumoniae* strains have been found around the world, e.g., in Colombia, Israel, and Brazil.[3,4] These resistant strains have emerged as virulent pathogens, and nosocomial infection is associated with high rates of mortality, as demonstrated in a recent, high-profile outbreak in the United States.[5]

While purine catabolism is relatively well understood and many of the enzymes involved have been biochemically and structurally characterized, important problems still remain unsolved in this area of metabolite catabolism.[6,7] Recently, a 23-gene cluster involved in a novel purine catabolic pathway was identified in *K. pneumoniae*.[8,9] Putative functions have been assigned for only 12 of these gene products and include enzymes, regulators, and transporters (Figure 1);[8,9] however, many of the gene products are still biochemically and structurally uncharacterized. Interestingly, *K. pneumoniae* appears to have a complete purine catabolic pathway that continues past allantoate to provide a nitrogen source for *K. pneumoniae*; however, the enzymatic activities responsible for the latter part of the pathway have not yet been assigned.[8] This pathway includes several enzymes that catalyze interesting chemical transformations, including HpxDE, a two-component oxygenase system that converts hypoxanthine to urate, HpxA, an allantoin racemase, and HpxO (Figure 1).

HpxO is the enzyme responsible for the conversion of uric acid to 5-hydroxyisourate.[10] This enzyme contains the $GxGxxG(x)_{17}E$ sequence motif and is therefore a member of the well-studied flavin adenine dinucleotide (FAD)-dependent glutathione reductase structural family.[11] Biochemical studies indicate that HpxO belongs to the class A flavin-dependent monooxygenase superfamily and requires FAD for activity.[10,12] These findings are in contrast to the mechanism of all other previously characterized urate oxidases, which proceed through direct reaction of an enzyme-stabilized urate dianion with triplet oxygen and do not require cofactors.[13−17]

Flavin-dependent monooxygenases are well-characterized.[18−20] HpxO, however, is the first example of an FAD-dependent urate oxidase. In this work, we report crystal structures of the unliganded and uric acid-bound forms of HpxO from *K. pneumoniae*. On the basis of the liganded structure, the R204Q variant was prepared and kinetically characterized. This change results in the uncoupling of the NADH oxidation and uric acid hydroxylation reactions. The structure of the R204Q variant suggests that this residue is involved in substrate activation for the transfer of oxygen from the flavin hydroperoxide. On the basis of these data, we propose a catalytic mechanism for flavin-mediated uric acid hydroxylation.

Received: September 14, 2012
Revised: December 21, 2012
Published: December 21, 2012

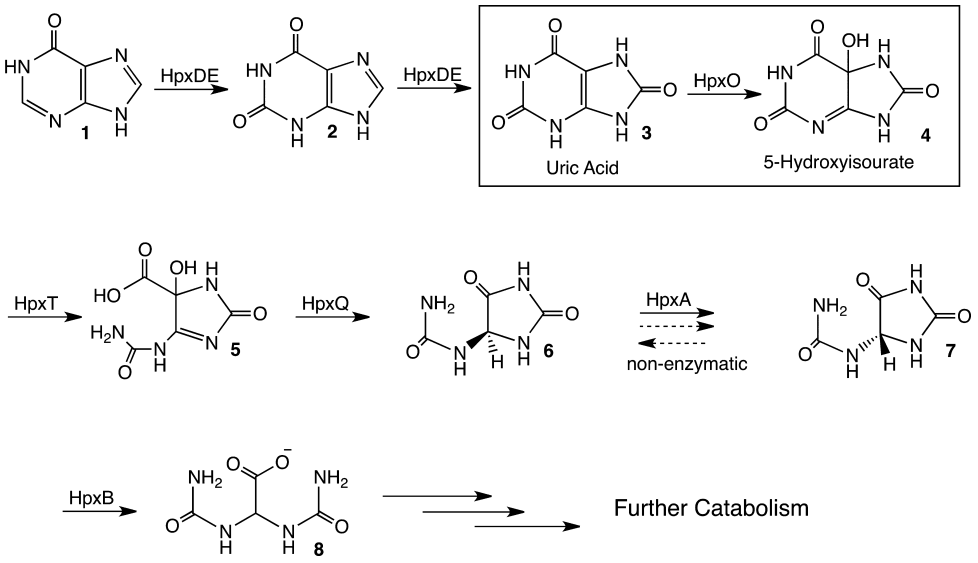

Figure 1. Purine degradation pathway in *K. pneumoniae*.

MATERIALS AND METHODS

Cloning of *K. pneumoniae* HpxO. Standard methods were used for DNA manipulations.[21,22] Plasmid DNA was purified with the Fermentas GeneJet miniprep kit, and DNA fragments were purified from agarose gel with the Zymoclean Gel DNA Recovery kit from Zymo Research. *Escherichia coli* strain MachI (Invitrogen) was used as a recipient for transformations during plasmid construction and for plasmid propagation and storage. Phusion DNA polymerase (New England Biolabs) was used for polymerase chain reactions (PCR) following the manufacturer's instructions. PfuTurbo DNA polymerase (Stratagene) was used for mutagenesis. All restriction enzymes were purchased from New England Biolabs. Plasmid THT is a derivative of pET-28, which was obtained from Novagen, and incorporates an N-terminal polyhistidine tag that can be cleaved by TEV protease and a short sequence to improve solubility.

The *hpxO* gene was amplified from *K. pneumoniae* genomic DNA (ATCC catalog no. 700721D) using standard PCR conditions and the following primer pair: 5′-GGG TAG CAT ATG AAA GCA ATC GTG ATT GGC GCC-3′ and 5′-CCC TAC TCG AGT TAG CCC AGC GGC CCG CTG AGG ATG G-3′. The amplified product containing the gene was excised from the gel, purified and digested with *Nde*I and *Xho*I, repurified, and ligated into similarly digested and purified pTHT. All PCR-derived DNA was sequenced to ensure that the PCR process had not introduced mutations. A correct clone was named HpxO.THT and transformed into *E. coli* strain B834(DE3) for overexpression.

Site-Directed Mutagenesis of HpxO. Mutagenesis was performed using a standard PCR-based protocol. Colonies were screened by colony PCR with a primer specific to the mutation and either the *T7* terminator primer or the *T7* promoter primer, which binds to the plasmid backbone. The sequences of the oligomeric primers used for site-directed mutagenesis are listed in the Supporting Information.

Production of Selenomethionyl (SeMet) HpxO. Overnight cultures were grown by the transfer of a single colony to 15 mL of LB medium supplemented with 25 μg/mL kanamycin at 37 °C while the cultures were being shaken for ∼16 h. The overnight cultures were pelleted by centrifugation at 4 °C for 15 min at 4000*g*. The resulting cell pellets were resuspended in 1 L of minimal medium supplemented with 1× M9 minimal salts, a concentration of 20 mg/L for all amino acids except methionine, 50 mg/L L-selenomethionine, 1× MEM vitamin mix, 0.4% glucose, 2 mM $MgSO_4$, 0.1 mM $CaCl_2$, 25 mg/L $FeSO_4$, and 25 μg/mL kanamycin. Cells were grown while being shaken at 37 °C. When cells reached an OD_{600} of 0.7−0.9, the temperature was lowered to 15 °C and overexpression of HpxO was induced by the addition of 1 mM isopropyl β-D-thiogalactopyranoside. After overnight growth with continued shaking (approximately ∼18 h), cells were pelleted by centrifugation at 4 °C for 15 min at 6000*g*. Cell pellets were stored at −80 °C until they were purified. Cells were resuspended in ∼25 mL of buffer A [20 mM Tris (pH 8), 500 mM NaCl, 30 mM imidazole, and 3 mM β-mercaptoethanol], and one complete mini EDTA-free protease inhibitor cocktail tablet (Roche) was added to the resuspended cells. Cells were lysed by sonication, and the cell lysate was cleared by centrifugation at 40000*g* for 45 min at 4 °C.

SeMet HpxO was purified from the clarified cell lysate by nickel affinity chromatography. The clarified lysate was loaded onto a 3 mL column pre-equilibrated with buffer A. The column was washed with ∼40 column volumes of buffer A and then washed with 5 column volumes of buffer A supplemented with 50 mM imidazole. SeMet HpxO was eluted from the column by addition of 5 column volumes of buffer A containing 250 mM imidazole. The protein was ∼95% pure as determined by sodium dodecyl sulfate−polyacrylamide gel electrophoresis (SDS−PAGE) analysis (results not shown). SeMet HpxO was then buffer exchanged into 10 mM Tris (pH 7.7), 30 mM NaCl, and 1 mM dithiothreitol (DTT) and concentrated to 7 mg/mL as determined by a Bradford assay.[23] One liter of culture produced approximately 14 mg of pure SeMet HpxO.

Overexpression and Purification of the R204Q HpxO Variant. The cells were grown and purified as previously described[10] except that riboflavin (0.05 g/L) was added to the culture medium. The protein was buffer exchanged by dialysis into 0.1 M potassium phosphate buffer (pH 8) for kinetic studies. For crystallographic studies, the protein was buffer exchanged into 10 mM Tris (pH 8) and 30 mM NaCl. All protein samples were purified to >90% as determined by SDS−

PAGE analysis. The purified protein was concentrated to 11 mg/mL.

Crystallization of HpxO and the R204Q Variant. Initial crystallization conditions were identified using the hanging drop vapor diffusion method (Crystal Screens 1 and 2, Hampton Research; Wizard Screens 1 and 2, Emerald Biosystems) at 18 °C. Hanging drops consisted of 1.5 μL of reservoir solution and 1.5 μL of protein solution. Optimized SeMet HpxO crystals were grown in the presence of 400 μL of reservoir solution consisting of 0.05 M KH_2PO_4 and 20% PEG 8000 with 150 μL of a 1:1 paraffin/silicone oil mixture over the surface of the reservoir. The addition of the paraffin/silicone oil mixture slowed crystal growth,[24] resulting in the formation of yellow needles that grew to 100−150 μm × 10−30 μm in 2 days. To obtain crystals of SeMet HpxO complexed with uric acid, SeMet HpxO crystals were transferred to a drop consisting of a saturated solution of uric acid in the reservoir solution and allowed to soak for ∼1.5 h at 18 °C. The crystallization buffer supplemented with 30% ethylene glycerol was used as the cryoprotectant. After being incubated in the cryoprotectant for 5 min, the sample was flash-frozen in liquid nitrogen. Both SeMet HpxO and the substrate complex crystals belong to space group $P2_12_12_1$. The asymmetric unit contains one monomer with a Matthews number of 2.7 Å^3/Da and a solvent content of 54%.

To ensure FAD binding, R204Q was incubated with 5 mM FAD at 4 °C for 2 h prior to crystallization. Drops were streak seeded using R204Q HpxO crystals grown in the absence of FAD. Crystals grew in 2 days at 18 °C in 0.2 M magnesium acetate, 0.1 M sodium cacodylate trihydrate (pH 6.5), and 20% PEG 8000. The crystallization buffer supplemented with 30% ethylene glycol was used as the cryoprotectant. Similar to wild-type HpxO, the R204Q variant belongs to space group $P2_12_12_1$.

X-ray Data Collection and Processing. Data were collected on a single SeMet HpxO crystal at NE-CAT beamline 24-ID-C at the Advanced Photon Source (Argonne National Laboratory, Argonne, IL) using a Quantum 315 detector (Area Detector Systems Corp.). To maximize the anomalous signal, a single-wavelength anomalous diffraction experiment was conducted at peak f'' for selenium. Data for the SeMet HpxO crystal were collected to 2.2 Å resolution using a 1° oscillation range over 260 frames. Data for the SeMet HpxO−uric acid complex were also collected to 2.0 Å resolution at beamline 24-ID-C, using a wavelength of 0.9791 Å, over 294 frames using a 1° oscillation range. Data were collected to 2.0 Å resolution for R204Q HpxO complexed with FAD at beamline 24-ID-C, using a wavelength of 0.9792 Å, over 120 frames using a 1° oscillation range. All data were indexed, integrated, and scaled using the HKL2000 suite of programs.[25] Table 1 summarizes the data collection statistics.

Structure Determination, Model Building, and Refinement. HpxO contains 11 methionine residues, and the initial SeMet positions were located using data cut off at 2.5 Å and hkl2map;[26,27] 10 of 11 SeMet residues were located. Initial electron density maps were calculated using these heavy atom sites, and automated model building was performed using SHARP/autoSHARP, which succeeded in modeling 162 residues with correct side chains and 114 residues as alanine residues of 385 total residues.[28] Initial refinement was conducted using Refmac 5.0[29] and the CCP4i interface.[30] Iterative rounds of manual model building were performed with COOT,[31] and later rounds of refinement were conducted using PHENIX.[32] During the later rounds of refinement, water molecules were added followed by the addition of an FAD molecule. Lastly, for the substrate complex, uric acid was modeled into HpxO prior to the final round of refinement. Geometry was verified using PROCHECK.[33] The refinement statistics are summarized in Table 2.

Table 1. Data Collection Statistics

	SeMet HpxO	SeMet HpxO−uric acid	R204Q HpxO
beamline	APS-24-ID-C	APS-24-ID-C	APS-24-ID-C
resolution (Å)	2.2	2.0	2.0
wavelength (eV)	12662.0	12662.5	12662.0
space group	$P2_12_12_1$	$P2_12_12_1$	$P2_12_12_1$
a (Å)	66.65	67.02	67.03
b (Å)	67.65	67.84	68.77
c (Å)	82.01	82.24	81.58
no. of measured reflections	157283	134891	119607
no. of unique reflections[a]	19184 (1781)[b]	24401 (2383)[b]	27220 (1308)[b]
average I/σ	22.7 (4.8)[b]	40.9 (8.6)[b]	27.3 (3.4)[b]
redundancy	8.2 (6.2)[b]	5.6 (5.5)[b]	4.4 (4.4)[b]
completeness (%)	98.4 (93.8)[b]	99.7 (99.3)[b]	99.4 (99.8)[b]
R_{sym}[c] (%)	10.0 (27.4)[b]	9.3 (31.1)[b]	4.8 (37.2)[b]

[a]Unique reflections include Bijvoet pairs. [b]Values in parentheses are for the highest-resolution shell. [c]$R_{sym} = \sum\sum_i|I_i - \langle I\rangle|/\sum\langle I\rangle$, where $\langle I\rangle$ is the mean intensity of N reflections with intensities I_i and common indices h, k, l.

Size Exclusion Chromatography. To determine the oligomeric state of the enzyme, SeMet HpxO was analyzed using analytical size exclusion chromatography (Superdex 200 10/300 GL, GE Healthcare). The column buffer consisted of 20 mM Tris (pH 8), 50 mM NaCl, and 1 mM DTT. Proteins with known oligomeric states were also prepared and used to

Table 2. Data Refinement Statistics

	SeMet HpxO	SeMet HpxO−uric acid	R204Q HpxO
resolution (Å)	34.9−2.20	33.9−2.04	48.0−1.97
no. of protein atoms	2924	2894	2902
no. of ligand atoms	53	65	54
no. of water atoms	61	194	112
no. of reflections in working set	19144	24336	25161
no. of reflections in test set	974	1229	1326
R factor[a] (%)	20.6	19.2	19.0
R_{free}[b] (%)	25.4	23.2	22.9
rmsd from ideals			
bonds (Å)	0.007	0.005	0.007
angles (deg)	1.029	1.035	1.082
average B factor (Å^2)	34.3	22.3	27.7
Ramachandran plot (%)			
most favored	90.7	91.0	91.6
additionally allowed	9.3	9.0	8.4
generously allowed	0	0	0
disallowed	0	0	0

[a]R factor = $\sum_{hkl}||F_{obs}| - k|F_{cal}||/\sum_{hkl}|F_{obs}|$, where F_{obs} and F_{cal} are observed and calculated structure factors, respectively. [b]For R_{free}, the sum is extended over a subset of reflections (5%) excluded from all stages of refinement.

dx.doi.org/10.1021/bi301262p | Biochemistry 2013, 52, 477−487

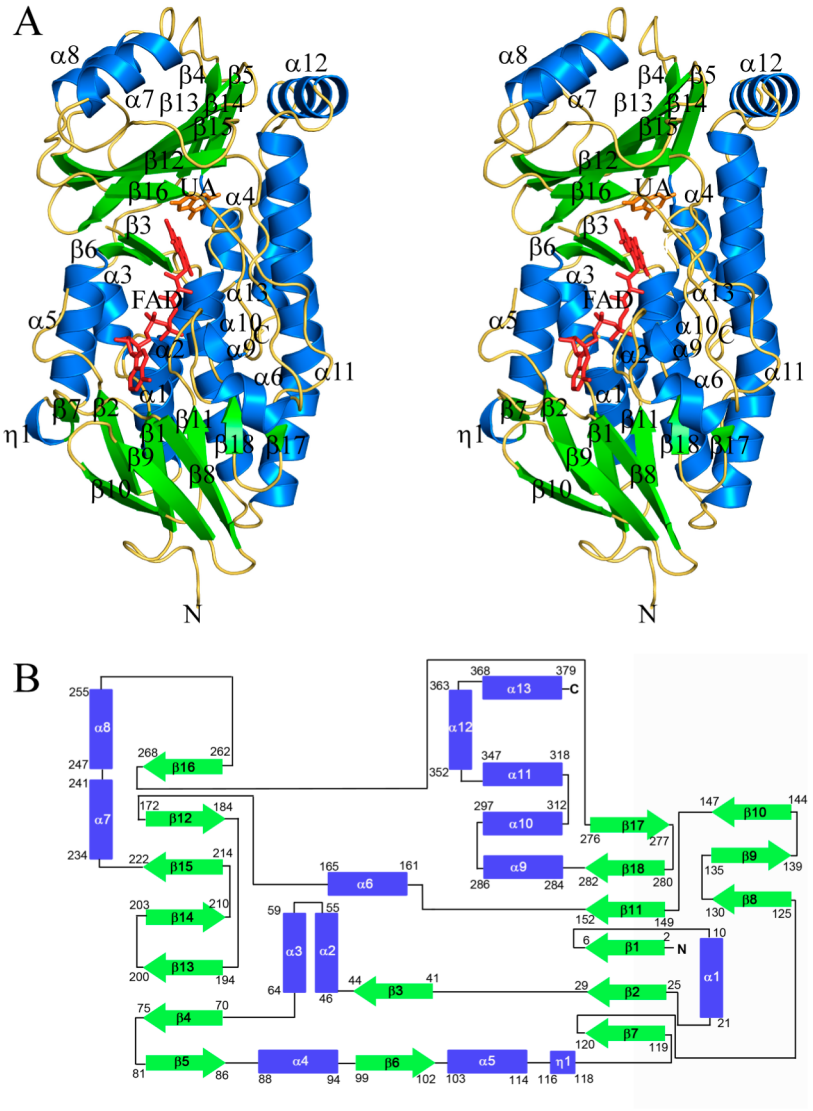

Figure 2. Structure of HpxO. (A) Stereoview ribbon diagram of HpxO with FAD and uric acid bound and secondary structural elements labeled. The α-helices are colored blue, the β-strands green, and the loops yellow. Ligands are shown as sticks. FAD is colored red, and uric acid is labeled as "UA" and colored orange. (B) Topology diagram of HpxO. The color scheme is the same as in panel A.

generate a standard curve of the partition coefficient (K_{av}) as a function of the log of the protein's molecular weight. On the basis of the measured K_{av} of SeMet HpxO, the protein is a monomer. All runs were performed at a flow rate of 0.5 mL/min at 4 °C.

Steady-State Kinetic Assays. For specific activity determinations, assays were conducted at 25 ± 1 °C in 0.1 M potassium phosphate buffer (pH 8.0), 10 mM NADH, 2 mM uric acid, and 1 mM FAD. The reaction product 5-hydroxyisourate spontaneously converts to allantoin on the time scale of the assay.[10] Stock solutions were prepared freshly in this buffer on the day of the assay. Absorbance measurements were recorded on a Cary 300 Bio UV−vis spectrophotometer (Varian). For analysis of NADH oxidation, an extinction coefficient of 0.75 mM^{-1} cm^{-1} at 385 nm was used. Protein concentrations were determined by the Bradford method.[23] We previously showed that the concentrations of wild-type HpxO could be determined reliably by this method.[10] For the calculation of V/E_o, the active protein concentration was assumed to be equal to the total protein concentration in the presence of 0.01 or 1 mM FAD.

For kinetic studies, the uric acid concentration was typically fixed at 1 mM in assays in which the NADH concentration was varied. When the uric acid concentration was varied, the NADH concentration was fixed at 1.5 mM. To minimize mixing effects, all other components of the HpxO reaction were typically added to the appropriate volume of the NADH stock solution to initiate the reaction. In a typical experiment, HpxO (final concentration of 100−900 nM), 0−1 mM uric acid, and 0.01 mM FAD were preincubated in 0.1 M potassium phosphate buffer and then added to an appropriate volume of 0−2 mM NADH to initiate the reaction. The reaction mixtures were then manually mixed prior to observing the absorbance change at 385 nm. The initial mixing step resulted in a delay of 12 ± 3 s between the initiation of the reaction and the acquisition of the first absorbance data point. The time domain for the absorbance data at each substrate concentration was chosen to produce the best linear fit to the initial change in 385 nm absorbance.

The absorbance data were analyzed by fitting the linear portions of the initial absorbance decay by linear least-squares regression to determine the rates of the change in absorbance at

dx.doi.org/10.1021/bi301262p | *Biochemistry* 2013, 52, 477−487

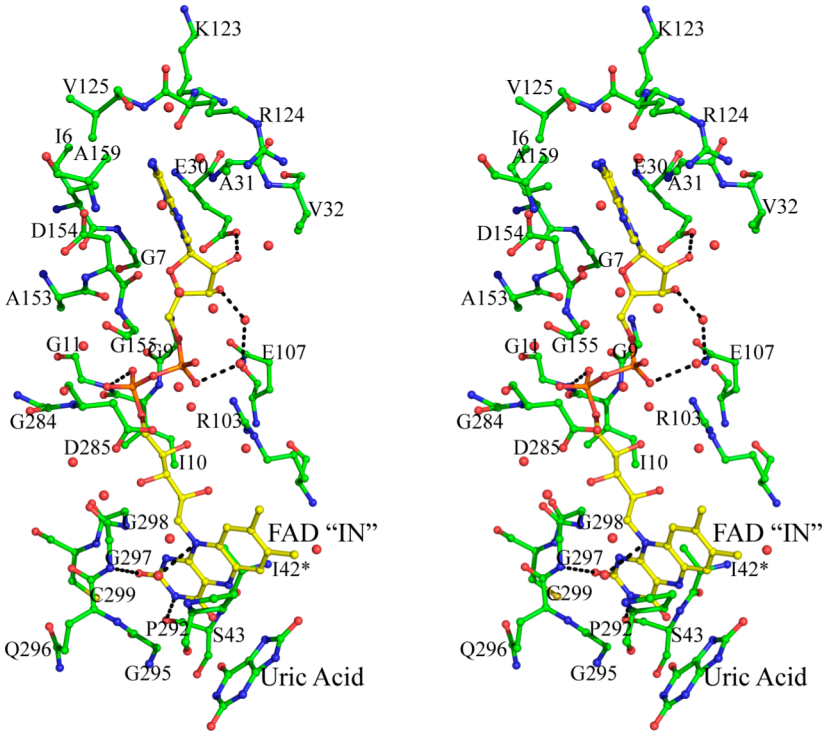

Figure 3. Stereoview diagram of the FAD binding site in HpxO with uric acid bound. The carbon residues in HpxO and uric acid are colored green using the ball-and-stick representation, and the interactions with the protein are indicated using dashed lines. Water molecules are shown as red nonbonded spheres. FAD adopts the *in* conformation and is shown with yellow carbon atoms. Clear electron density is not seen for the side chain of Ile42, which is labeled as I42*.

385 nm as a function of initial substrate concentration. These rates were converted to rates of change in NADH concentration and plotted as a function of $[NADH]_o$. The resulting data were fit by nonlinear regression to the Michaelis–Menten equation. Regression analysis was conducted using Grafit 5.0 (Erithacus Software). The kinetic constants were determined on the basis of at least two independent experiments. The standard errors reported in the text are the standard errors to the linear or nonlinear fits.

High-Performance Liquid Chromatography (HPLC) Analysis of the Products of the HpxO-Catalyzed Reaction. All reactions were assayed by reverse-phase HPLC on an Agilent 1100 HPLC system equipped with a quaternary pump and a 1.0 mL sample loop. The system also had a diode array UV–vis detector (190–640 nm) and a fluorescence detector. The stationary phase was a Supelcosil LC-18-T column (15 cm × 4.6 mm, 3 μm particles), maintained at room temperature (21 ± 1 °C). At the end of the incubation period for the enzymatic reaction, the protein was removed by centrifugal ultrafiltration of the reaction mixture (10 kDa molecular mass cutoff membrane). Aliquots of 0.02–0.05 mL of the filtrate were then removed and analyzed for urate and allantoin. The LC eluent consisted of a gradient of methanol in 10 mM potassium phosphate buffer (pH 6.6). In the analytical method, percentages P and M of phosphate buffer and methanol (balance water), respectively, at time t (in min) varied according to the following scheme: [t,P,M]: [0,100,0], [4,90,0], [9,60,15], [14,10,65], [16,100,0], [21,100,0].

Figure Preparation. Figures were generated using PyMOL[34] and ChemBioDraw (CambridgeSoft).

RESULTS

Structure of the HpxO Monomer. The asymmetric unit contains one monomer of HpxO, and the final model contains residues 1–36 and 40–384 of the protein chain, eight residues of the polyhistidine tag spacer, and one molecule of FAD. The substrate complex also contained one molecule of uric acid. A disordered region consisting of residues 37–39 was missing in the electron density and was therefore not included in the final model. This region is near a cavity leading to the HpxO active site. The final model is shown in Figure 2. HpxO is structurally similar to other flavin-dependent monooxygenases and consists of three domains. The N-terminal domain has a six-stranded mainly parallel β-sheet (β7↑β2↑β1↑β11↑β18↑β17↓) flanked on one side by a three-stranded antiparallel β-sheet (β8↑β9↓β10↑) and one α-helix and on the other side by five α-helices, a two-stranded antiparallel β-sheet (β6↓, β13↑), and a small 3_{10}-helix. The N-terminal domain forms most of the interactions with the FAD molecule. The second domain consists of a seven-stranded mostly antiparallel β-sheet (β5↓β4↑β13↑β14↓β15↑ β12↓β16↑) that is flanked by two α-helices that are solvent-exposed. This domain forms part of the uric acid binding pocket. Finally, the C-terminal domain connects the first two domains. It consists of a long α-helix (α11) that stretches the length of HpxO and four shorter α-helices (α9, α10, α12, and α13). On the basis of size exclusion chromatography, HpxO is also a monomer in solution (data not shown).

FAD Binding Site. One FAD molecule binds to the HpxO monomer in an extended conformation in a cavity that is approximately 24 Å long and 9–15 Å wide. In the wild-type HpxO structures obtained in the presence and absence of uric acid, the FAD is found in the *in* conformation (Figure 3).[35] Mostly hydrophobic residues surround the FAD, including Ile6,

dx.doi.org/10.1021/bi301262p | *Biochemistry* 2013, 52, 477–487

Val32, Lys123, Arg124, Val125, Asp154, Gly155, and Ala159 for the adenine base and Gly7, Ala31, and Ala153 for the ribose sugar. The 2′-hydroxyl group of the ribose ring forms a hydrogen bond with the carboxylate group of Glu30, and the 3′-hydroxyl forms a water-mediated hydrogen bond to Gln107. The α-phosphate group forms a hydrogen bond to a water molecule, while the β-phosphate group interacts with the backbone amide nitrogen atom of Gly11. Other residues near this region include Gly9, Ile10, Arg103, Gly284, and Asp285. The isoalloxazine ring is located in a binding pocket containing primarily hydrophobic residues, including Ile42, Pro292, Gly298, and Cys299. The carbonyl oxygen atom of C2 makes a hydrogen bond to the backbone amide nitrogen atom of Gly297. N3 is hydrogen bonded to the carbonyl oxygen atoms of Ser43, and N10 forms a hydrogen bond to a water molecule.

Substrate Binding Site. To obtain the liganded complex, we soaked uric acid into SeMet HpxO by incubating the crystals for ∼1.5 h at 18 °C with a reservoir solution consisting of a saturated solution of uric acid. Uric acid binds to HpxO in a pocket with an average dimension of ∼10 Å. As shown in Figure 4, a channel ∼9 Å wide and ∼20 Å long, containing

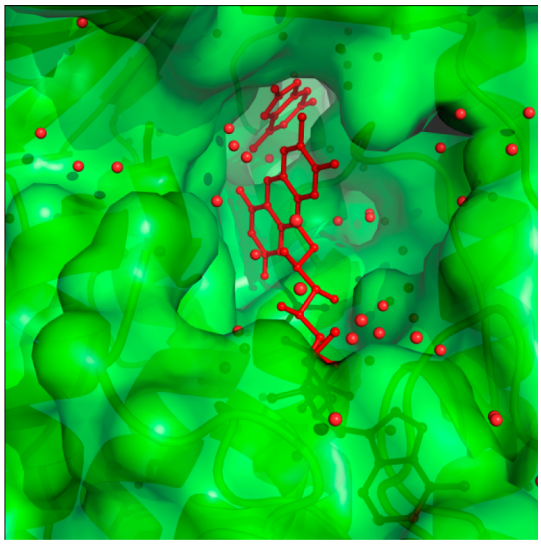

Figure 4. Space filling model of HpxO showing the substrate tunnel leading to the active site. FAD and uric acid are colored red and shown as balls and sticks. Water molecules are shown as red spheres. The surface of HpxO is colored green, and the secondary structure elements are shown as cartoons.

mainly hydrophobic and aromatic residues, allows entry of the uric acid into the active site. The uric acid binding site and electron density are shown in panels A and B of Figure 5, respectively. As shown in Figure 5A, the hydroxyl group on C6 of uric acid is 2.8 Å from the hydroxyl group at C4 of the isoalloxazine ring. The uric acid binding pocket is lined with aromatic residues, including Phe218, which forms a $\pi-\pi$ stacking interaction with uric acid, Tyr216, which forms a hydrogen bond to the oxygen atom on C8 of uric acid, Tyr195, Tyr216, Phe218, Trp45, and Trp195. A number of charged residues are also found in the active site, including most notably Arg204, which forms hydrogen bonds with both the amide nitrogen (N3) and oxygen at C2 of urate. Other charged residues in the uric acid binding pocket are Asn178, Asp220, and Asp293. A number of nonpolar amino acid residues, including Met208, Pro292, Ile294, and Gly295, are also located in the uric acid binding pocket.

R204Q HpxO Variant Structure. Because of the significant effect of the R204Q variant on catalysis (Table 3), crystals of HpxO containing the R204Q mutation were obtained in the presence of FAD. The asymmetric unit contains one monomer of R204Q HpxO, and the final model contains residues 1−35 and 40−384 of the protein chain, one residue of the His_6 tag, and one molecule of FAD. Residues 36−39 form a flexible loop region, which is missing from the electron density and thus is not included in the final model. The overall fold of R204Q HpxO is the same as that of the wild type (Figure 2) and also consists of three domains. One FAD molecule binds to the R204Q HpxO monomer in an extended conformation. As shown in Figure 6, the FAD adopts the *in* conformation in the R204Q structure. FAD is also in the *in* conformation in the wild-type HpxO structures determined in the presence or absence of uric acid (Figure 3). Attempts to crystallize the R204Q HpxO−uric acid−FAD complex produced crystals that diffracted to >6 Å resolution and decayed rapidly because of radiation damage, thus preventing structural analysis. The residues in the FAD binding site in R204Q adopt the same conformation as in the wild-type binding site, with the exception of Arg103 (Figures 3 and 6).

Steady-State Kinetic Analysis. To interrogate the roles of R204 and Y216 in catalysis, we measured the steady-state kinetics of NADH oxidation for the R204Q and Y216F variants of HpxO (Table 3). The R204Q mutant catalyzed slow oxidation of NADH with a rate that was unaltered by the presence of urate (k_{cat} ∼ 0.25 s^{-1}); this rate is comparable with that of the wild-type enzyme in the absence of urate. Low levels of allantoin formation could be observed upon extended incubation of R204Q HpxO with urate and NADH in the presence of FAD, but the rate and extent of this reaction were too low to allow construction of a Michaelis−Menten plot for urate. The $K_{m,NADH}$ for NADH oxidation catalyzed by R204Q HpxO was increased slightly (640 μM) in comparison with that of the wild-type enzyme (500 μM). The ∼10^4-fold reduction in $k_{cat}/K_{m,NADH}$ is entirely a consequence of the reduced k_{cat} value.

In contrast, the Y216F variant exhibited measurable but significantly reduced activity ($k_{cat}/K_{m,urate}$ that is ∼10% of that of the wild-type enzyme). The K_m for urate was doubled, while the K_m for NADH was decreased 5-fold relative to that of the wild-type enzyme, to 100 μM for Y216F HpxO. Thus, while $k_{cat}/K_{m,urate}$ is one order of magnitude lower for this variant than for the wild-type enzyme, $k_{cat}/K_{m,NADH}$ is essentially unchanged, decreasing from 0.125 to 0.084 μM^{-1} s^{-1}.

DISCUSSION

Comparison of HpxO with Other Enzymes. Recent biochemical characterization confirmed that HpxO is a member of the flavin monooxygenase family and requires one molecule of FAD for optimal activity.[10] On the basis of analysis using the DALI structure server,[36] the five closest structural homologues to HpxO are listed in Table 4. These enzymes are 2,6-dihydroxypyridine 3-hydroxylase (DHPH), 2-methyl-3-hydroxypyridine-5-carboxylic acid oxygenase (MHPCO), *p*-hydroxybenzoate hydroxylase (PHBH), phenol hydroxylase, and 3-hydroxybenzoate hydrolase (MHBH). The rmsd for each of these enzymes with respect to HpxO is <3.2 Å for at least 360 aligned residues with Z scores of ≥21.0. A flavin-dependent monooxygenase similar to HpxO, but involved in the metabolism of caffeine by *Pseudomonas* sp. strain CBB1, was

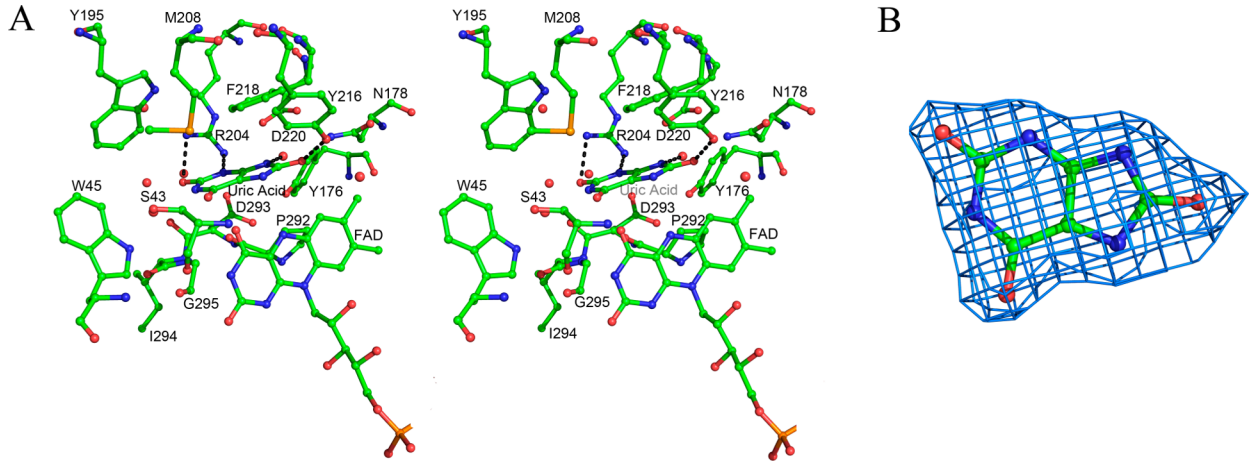

Figure 5. Uric acid binding site. (A) Stereoview diagram of the active site of HpxO with FAD and uric acid bound. Water molecules are shown as nonbonded red spheres. Hydrogen bonds between uric acid and HpxO are shown as dashed lines. (B) Composite omit density shown around the uric acid at a contour level of 3σ (blue).

Table 3. Kinetic Parameters for HpxO Active Site Variants

Enzyme	k_{cat} (s^{-1})	$K_{m,urate}$ (μM)	$K_{m,NADH}$ (μM)	$k_{cat}/K_{m,urate}$ (μM^{-1} s^{-1})	$k_{cat}/K_{m,NADH}$ (μM^{-1} s^{-1})
Wild-Type	42 ± 2	42 ± 8	~500	1.0 ± 0.2	0.125 ± 0.030
R204Q	0.26 ± 0.006	ND[a]	640 ± 39	ND[a]	~10^{-4}
Y216F	8.4 ± 0.5	90 ± 20	100 ± 35	0.093 ± 0.021	0.084 ± 0.030

[a]Not determined.

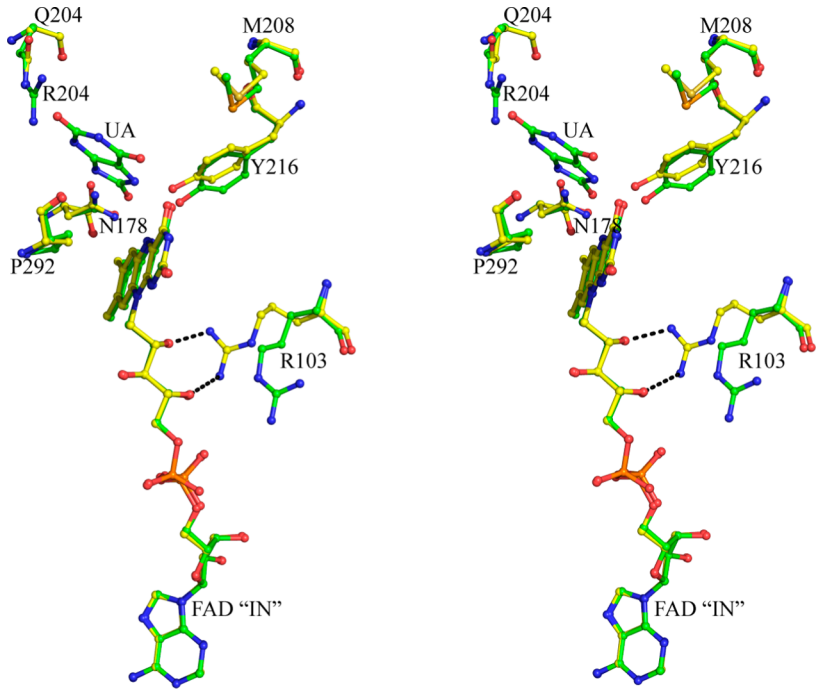

Figure 6. Stereoview comparison of the active sites of R204Q HpxO and wild-type HpxO. Amino acid residues and ligands are shown using a ball-and-stick representation in which carbon atoms in the wild-type HpxO structure are colored green and those in the R204Q structure are colored yellow. Residues and ligands are shown using the ball-and-stick representation using the same color scheme. Interactions with the protein are indicated by dashed lines. In the wild-type structure, there is a SeMet at position 208.

recently identified; this enzyme catalyzes the conversion of 1,3,7-trimethyluric acid to 1,3,7-trimethyl-5-hydroxyisouric acid but differs in its substrate binding pocket and does not catalyze monooxygenation of uric acid.[37]

The FAD binding site is well-conserved among members of the class A flavin monooxygenase superfamily.[12,35,38−41] In HpxO, the adenine ring of FAD is bound between an arginine residue (Arg124) and an aspartate residue (Asp154). Conserved residues in the FAD binding pocket include Glu30, which is oriented toward the hydroxyl groups of the ribose ring, and Gly7, Gly11, and Asp285.[39,40] On the basis of previous structural studies of other flavin monooxygenases,

dx.doi.org/10.1021/bi301262p | *Biochemistry* 2013, 52, 477−487

Table 4. Enzymes Identified as Structurally Similar to HpxO Based on DALI

protein	PDB entry	Z score	rmsd	% identical	no. of aligned residues
2,6-dihydroxypyridine 3-hydroxylase (DHPH)	2VOU	37.9	2.3	22	347
2-methyl-3-hydroxypyridine-5-carboxylic acid (MHPCO)	3GMC	37.6	2.6	19	339
p-hydroxybenzoate hydroxylase (PHBH)	1YKJ	34.4	3.0	15	360
phenol hydroxylase	1FOH	31.5	2.9	16	346
3-hydroxybenzoate hydrolase (MHBH)	2DKH	21.0	3.2	16	338

including most notably PHBH and RebC, the isoalloxazine ring of FAD adopts three main conformations: *in*, *open*, and *out*. During the catalytic reaction, reduction of FAD by NADH occurs in the *out* site and hydroperoxyflavin-mediated substrate hydroxylation occurs in the *in* site.[35,42,43] In the *open* conformation, the flavin occupies the *in* site, but the substrate is not bound. The change in conformation from *in* to *out* requires ∼7−8 Å of FAD movement and is usually enhanced by substrate binding. In all HpxO structures obtained (liganded, unliganded, and R204Q), the FAD molecule binds lengthwise in an extended conformation with the isoalloxazine ring adopting the *in* conformation (Figures 3 and 6).

The NADH binding site is also well-conserved among members of the class A flavin monooxygenase superfamily.[12] The NADH binding site has not been identified in HpxO; however, structural alignment of the HpxO−uric acid complex with R220Q PHBH (PDB entry 1K0J)[44] identifies a groove near the surface of HpxO where NADH could bind. However, C4 on the nicotinamide ring is ∼20 Å from N5 of the flavin, suggesting that for reduction of the flavin to take place there must be movement of the flavin to the *out* conformation and also movement of the NADH.[44] This movement would ensure that FAD reduction occurs on the *re* face of the isoalloxazine ring.[35] However, similar to MHPCO, the FAD conformation in HpxO is in the *in* conformation irrespective of the presence or absence of substrate.[40] Manual modeling of the flavin C4a-hydroperoxide intermediate into the HpxO active site indicates that the terminal oxygen of the hydroperoxide intermediate is approximately 3.4 Å from C5 of uric acid (data not shown), indicating that the substrate and cofactor are well-positioned to react.

The mechanism of substrate binding differs widely for the flavin monooxygenases.[39−41] HpxO contains a tunnel, mainly comprised of hydrophobic and aromatic residues, which we hypothesize allows for uric acid binding (Figure 4). The opening to this tunnel is a disordered loop region (residues

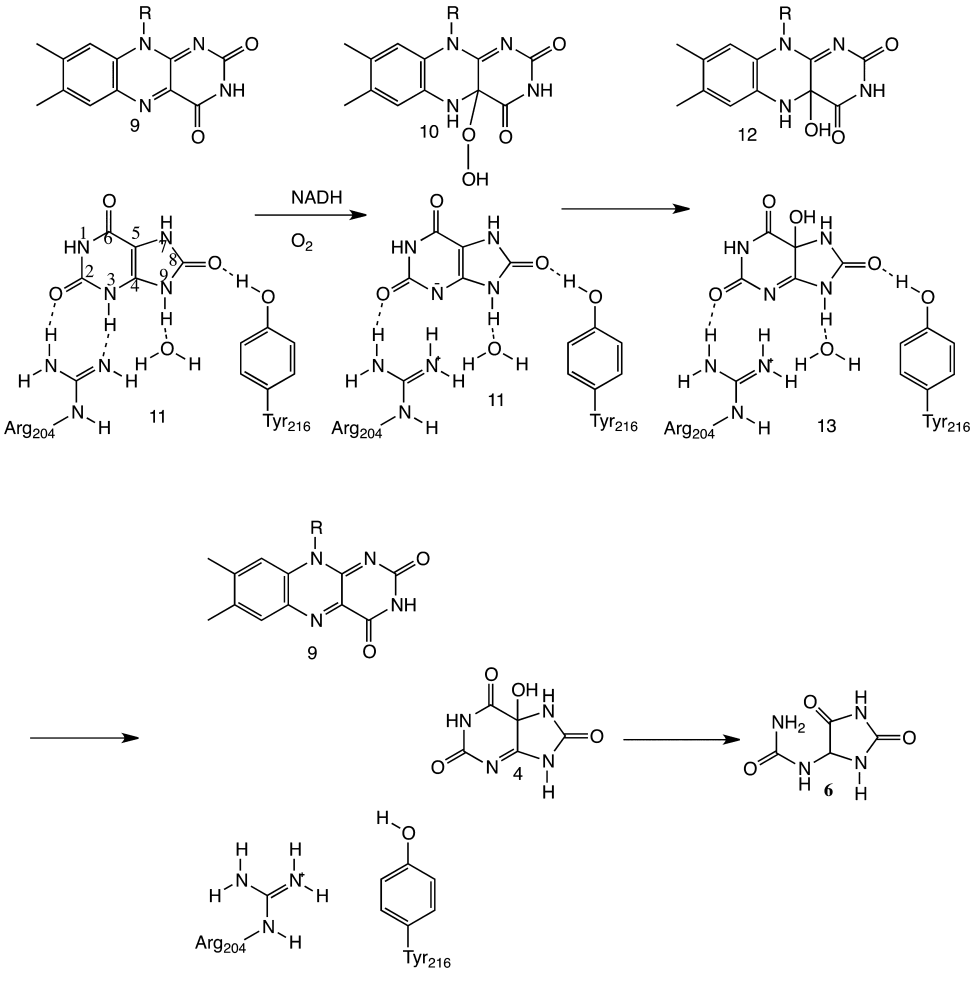

Figure 7. Proposed mechanism for the HpxO-catalyzed reaction.

dx.doi.org/10.1021/bi301262p | *Biochemistry* 2013, 52, 477−487

37−39), which was not present in the HpxO electron density. It appears that this loop region could control tunnel access. The loop remains disordered in the HpxO−uric acid complex, consistent with the idea that assembly of the HpxO-FAD-urate-NADH complex is required prior to closure of the active site. This region aligns with a similar flexible loop in phenol hydroxylase (PDB entry 1FOH). In the phenol hydroxylase reaction, this loop moves during catalysis to accommodate changes in FAD conformation.[38]

As shown in Figure 5A, the active site of HpxO contains aromatic, nonpolar, and charged residues. The aromatic residues include Trp45, Tyr195, Tyr216, and Phe218. The large number of aromatic residues in the HpxO active site is not surprising, as other flavin monooxygenases also contain many aromatic residues, some of which are involved in $\pi-\pi$ stacking interactions.[45] The nonpolar residues in the HpxO active site are Met208, Pro292, Ile294, and Gly295, and the charged residues include Asn178, Arg204, Asp220, and Asp293. Another common feature of the active sites of flavin monooxygenases is a conserved proline residue above the FAD isoalloxazine ring; this residue is Pro292 in HpxO.

The main interactions between HpxO and uric acid involve Arg204, which forms hydrogen bonds with both O2 and N3 of uric acid. An additional hydrogen bond is formed between the hydroxyl group of Tyr216 and O8 of uric acid. These interactions are important for both proper substrate orientation and catalysis (see below).

Comparison of Wild-Type and R204Q HpxO Structures. The conformations of the residues in the FAD binding site of HpxO are largely identical in the wild-type and R204Q structures, with the exception of Arg103, which moves approximately 3.4 Å between the two structures (Figure 6). In the R204Q structure, the guanidinium group on Arg103 is pointed directly toward the hydroxyl groups on the ribityl side chain of FAD and forms a salt bridge to the hydroxyl groups on C2 and C4. In the wild-type structure, the guanidinium group of Arg103 is pointed away from the FAD and the distance between the guanidinium group and the hydroxyl on C2 is >6 Å. However, we cannot rule out the possibility that the altered conformation of Arg103 could be caused by differences in the crystallization conditions of the wild-type enzyme versus the R204Q variant. Minor changes are also seen in the conformation of Asn178.

The conformations of the residues in the uric acid binding site are similar in the wild-type and R204Q HpxO structures. The most significant change is in the position of Tyr216, which in the R204Q structure resides closer to the uric acid binding pocket by approximately ∼1.9 Å (Figure 6). Minor changes in the positions of Met208 and Pro292 are also observed.

Uncoupled NADH Oxidation with HpxO R204Q. The purified R204Q variant exhibited lower FAD occupancy than wild-type HpxO but could be quantitatively reconstituted by incubation with 0.01 mM FAD. The excess cofactor was then removed by gel filtration.

Steady-state kinetic studies of HpxO R204Q indicated that the presence of uric acid had no effect on the steady-state kinetics of oxidation of NADH. The K_m value for NADH was close to the value for the wild-type enzyme in the presence of saturating concentrations of urate, and the k_{cat} value was 160 times slower than that of the wild-type enzyme.

Mechanistic Implications. A mechanistic proposal for the HpxO-catalyzed oxidation of uric acid by the flavin hydroperoxide is shown in Figure 7. Structure **11** shows the interactions between the enzyme and the uric acid substrate. Arg204 deprotonates N3 of the substrate and stabilizes the resulting anion by hydrogen bonding to the C2 carbonyl. A similarly positioned and highly conserved arginine residue is observed in the crystal structure of cofactor-independent urate oxidase bound to a urate analogue,[46] where urate deprotonation to form the dianion is critical for substrate activation. In addition to forming hydrogen bonds with urate, Arg204 forms a hydrogen bond to Asp220, which in turn hydrogen bonds to His348. Asp293 bridges His348 and Tyr176, and a water molecule joins Tyr176 and Arg204. This unusual hydrogen bonding network is otherwise mostly buried in a hydrophobic region near the active site and may be responsible for lowering the pK_a of Arg204. An active site water is hydrogen bonded to N9, and Tyr216 is hydrogen bonded to the C8 carbonyl anchoring the substrate in the active site. The negative charge on N3 is delocalized onto C5, enhancing the nucleophilicity of this carbon for attack on flavin hydroperoxide **10** to give **12** and **13**. Product dissociation and loss of water from hydroxyflavin **12** complete the formation of 5-hydroxyisourate **4**, which spontaneously converts to allontoin **6** under the assay conditions.[10] Active site mutagenesis studies are consistent with the proposed roles for Arg204 and Tyr216 (Table 3). The Y216F variant shows small effects on catalysis consistent with a role in substrate binding rather than N9 deprotonation. In contrast, the k_{cat} for the R204Q variant was 160-fold lower than that for wild-type HpxO, while $K_{m,NADH}$ increased slightly, consistent with an important function in substrate activation by deprotonation. In addition, the NADH oxidase activity of the R204Q variant was independent of added uric acid and comparable with wild-type NADH oxidase activity in the absence of urate, suggesting that without substrate deprotonation, oxygen transfer does not occur efficiently. A small amount of allantoin could be detected after extended incubation of the R204Q variant with urate and NADH, consistent with the proposal that the variant enzyme can catalyze both NADH oxidation and urate hydroxylation but that the coupling between the two reactions is eliminated.

In summary, our structural and biochemical characterizations of HpxO provide new mechanistic insights into the first example of an FAD-dependent urate oxidase and suggest a new mechanism for the conversion of urate to 5-hydroxyisourate.

■ ASSOCIATED CONTENT

Supporting Information

Sequences of the oligomeric primers used for site-directed mutagenesis. This material is available free of charge via the Internet at http://pubs.acs.org.

Accession Codes

The Protein Data Bank codes for HpxO, the HpxO−uric acid complex, and the R204Q variant are 3RP6, 3RP7, and 3RP8, respectively.

■ AUTHOR INFORMATION

Corresponding Author

*Department of Chemistry and Chemical Biology, Cornell University, Ithaca, NY 14853. Telephone: (607) 255-7961. Fax: (607) 255-1227. E-mail: see3@cornell.edu (S.E.E.) or begley@chem.tamu.edu (T.P.B.).

Funding

This research was supported by a grant from the National Institutes of Health (GM073220 to S.E.E.) and by the Robert A. Welch Foundation (Grant A-0034 to T.P.B.).

Notes

The authors declare no competing financial interest.

■ ACKNOWLEDGMENTS

We thank the staff scientists at the APS NE-CAT beamlines for their assistance in data collection. Dr. Cynthia Kinsland of the Cornell Protein Production facility is thanked for providing clones of HpxO and the variant enzymes. We also thank members of the Ealick laboratory for comments on and editing of the manuscript. Dr. Yang Zhang is acknowledged and thanked for helpful discussions about this work. Leslie Kinsland's assistance during manuscript preparation is greatly appreciated. This work is based upon research conducted at the Advanced Photon Source on the Northeastern Collaborative Access Team beamlines, which are supported by Grant RR-15301 from the National Center for Research Resources at the National Institutes of Health. Use of the Advanced Photon Source is supported by the U.S. Department of Energy, Office of Basic Energy Sciences, under Contract DE-AC02-06CH11357.

■ ABBREVIATIONS

FAD, flavin adenine dinucleotide; SeMet, selenomethionyl; Tris, tris(hydroxymethyl)aminomethane base; DTT, dithiothreitol; UA, uric acid; DHPH, 2,6-dihydroxypyridine 3-hydroxylase; MHPCO, 2-methyl-3-hydroxypyridine-5-carboxylic acid oxygenase; PHBH, *p*-hydroxybenzoate hydroxylase; MHBH, 3-hydroxybenzoate hydrolase; DHP, 2,6-dihydroxypyridine; PDB, Protein Data Bank; rmsd, root-mean-square deviation.

■ REFERENCES

(1) Vanwynsberghe, T., Verhamme, K., Raymaekers, M., Cartuyvels, R., Van Vaerenbergh, K., Boel, A., and de Beenhouwer, H. (2009) A Large Hospital Outbreak of *Klebsiella pneumoniae* (DHA-1 and SHV-11 Positive): Importance of Detection and Treatment of ampC -Lactamases. *Open Infect. Dis. J. 3*, 55−60.

(2) Ko, W.-C., Paterson, D. L., Sagnimeni, A. J., Hansen, D. S., Von Gottberg, A., Mohapatra, S., Casellas, J. M., Goossens, H., Mulazimoglu, L., Trenholme, G., Klugman, K. P., McCormack, J. G., and Yu, V. L. (2002) Community-Acquired *Klebsiella pneumoniae* Bacteremia: Global Differences in Clinical Patterns. *Emerging Infect. Dis. 8*, 160−166.

(3) Maltezou, H. C. (2009) Metallo-*β*-lactamases in Gram-negative bacteria: Introducing the era of pan-resistance? *Int. J. Antimicrob. Agents 33*, 405.e401−405.e407.

(4) Nordmann, P., Cuzon, G., and Naas, T. (2009) The real threat of *Klebsiella pneumoniae* carbapenemase-producing bacteria. *Lancet 9*, 228−236.

(5) Snitkin Evan, S., Zelazny Adrian, M., Thomas Pamela, J., Stock, F., Henderson David, K., Palmore Tara, N., and Segre Julia, A. (2012) Tracking a Hospital Outbreak of Carbapenem-Resistant *Klebsiella pneumoniae* with Whole-Genome Sequencing. *Science Translational Medicine 4*, 148ra116.

(6) Zrenner, R., Stitt, M., Sonnewald, U., and Boldt, R. (2006) Pyrimidine and Purine Biosynthesis and Degradation in Plants. *Annu. Rev. Plant Biol. 57*, 805−836.

(7) Vogels, G. D., and Van der Drift, C. (1976) Degradation of purines and pyrimidines by microorganisms. *Bacteriol. Rev. 40*, 403−468.

(8) de la Riva, L., Badia, J., Aguilar, J., Bender, R. A., and Baldoma, L. (2008) The hpx Genetic System for Hypoxanthine Assimilation as a Nitrogen Source in *Klebsiella pneumoniae*: Gene Organization and Transcriptional Regulation. *J. Bacteriol. 190*, 7892−7903.

(9) Pope, S. D., Chen, L.-L., and Stewart, V. (2009) Purine Utilization by *Klebsiella oxytoca* M5al: Genes for Ring-Oxidizing and -Opening Enzymes. *J. Bacteriol. 191*, 1006−1017.

(10) O'Leary, S. E., Hicks, K. A., Ealick, S. E., and Begley, T. P. (2009) Biochemical Characterization of the HpxO Enzyme from *Klebsiella pneumoniae*, a Novel FAD-Dependent Urate Oxidase. *Biochemistry 48*, 3033−3035.

(11) Dym, O., and Eisenberg, D. (2001) Sequence-structure analysis of FAD-containing proteins. *Protein Sci. 10*, 1712−1728.

(12) van Berkel, W. J. H., Kamerbeek, N. M., and Fraaije, M. W. (2006) Flavoprotein monooxygenases, a diverse class of oxidative biocatalysts. *J. Biotechnol. 124*, 670−689.

(13) Busi, E., Terzuoli, L., Basosi, R., Porcelli, B., and Marinello, E. (2004) EPR Spin Trapping of a Radical Intermediate in the Urate Oxidase Reaction. *Nucleosides, Nucleotides Nucleic Acids 23*, 1131−1134.

(14) Kahn, K., and Tipton, P. A. (1997) Kinetic Mechanism and Cofactor Content of Soybean Root Nodule Urate Oxidase. *Biochemistry 36*, 4731−4738.

(15) Tipton, P. A. (2002) Urate oxidase: Single-turnover stopped-flow techniques for detecting two discrete enzyme-bound intermediates. *Methods Enzymol. 354*, 310−319.

(16) Imhoff, R. D., Power, N. P., Borrok, M. J., and Tipton, P. A. (2003) General Base Catalysis in the Urate Oxidase Reaction: Evidence for a Novel Thr-Lys Catalytic Diad. *Biochemistry 42*, 4094−4100.

(17) Sarma, A. D., and Tipton, P. A. (2000) Evidence for Urate Hydroperoxide as an Intermediate in the Urate Oxidase Reaction. *J. Am. Chem. Soc. 122*, 11252−11253.

(18) Harayama, S., Kok, M., and Neidle, E. L. (1992) Functional and Evolutionary Relationships Among Diverse Oxygenases. *Annu. Rev. Microbiol. 46*, 565−601.

(19) Torres Pazmino, D. E., Winkler, M., Glieder, A., and Fraaije, M. W. (2010) Monooxygenases as biocatalysts: Classification, mechanistic aspects and biotechnological applications. *J. Biotechnol. 146*, 9−24.

(20) Fagan, R. L., and Palfey, B. A. (2010) Flavin-Dependent Enzymes. In *Comprehensive Natural Products II* (Lew, M., and Hung-Wen, L., Eds.) Vol. 7, Section 7.03, pp 37−113, Elsevier, Oxford, U.K.

(21) Ausubel, F. M., Brent, R., Kingston, R. E., Moore, D. D., Seidman, J. G., Smith, J. A., and Struhl, K. (2002) *Short Protocols in Molecular Biology*, 5th ed., John Wiley and Sons, Chichester, U.K.

(22) Maniatis, T., Fritsch, E. F., and Sambrook, J. (1982) *Molecular Cloning: A Laboratory Manual*, Cold Spring Harbor Laboratory Press, Plainview, NY.

(23) Bradford, M. M. (1976) A rapid and sensitive method for the quantitation of microgram quantities of protein utilizing the principle of protein-dye binding. *Anal. Biochem. 72*, 248−254.

(24) Chayen, N. (1997) A novel technique to control the rate of vapour diffusion, giving larger protein crystals. *J. Appl. Crystallogr. 30*, 198−202.

(25) Otwinowski, Z., Minor, W., and Carter, C. W., Jr. (1997) Processing of X-ray diffraction data collected in oscillation mode. In *Methods in Enzymology*, pp 307−326, Academic Press, San Diego.

(26) Pape, T., and Schneider, T. R. (2004) HKL2MAP: A graphical user interface for phasing with SHELX programs. *J. Appl. Crystallogr. 37*, 843−844.

(27) Schneider, T. R., and Sheldrick, G. M. (2002) Substructure solution with SHELXD. *Acta Crystallogr. D58*, 1772−1779.

(28) Vonrhein, C., Blanc, E., Roversi, P., and Bricogne, G. (2007) Automated structure solution with autoSHARP. *Methods Mol. Biol. 364*, 215−230.

(29) Murshudov, G. N., Vagin, A. A., Lebedev, A., Wilson, K. S., and Dodson, E. J. (1999) Efficient anisotropic refinement of macromolecular structures using FFT. *Acta Crystallogr. D55*, 247−255.

(30) Collaborative Computational Project Number 4 (1994) The CCP-4 suite: Programs for protein crystallography. *Acta Crystallogr. D50*, 760−763.
(31) Emsley, P., and Cowtan, K. (2004) Coot: Model-building tools for molecular graphics. *Acta Crystallogr. D60*, 2126−2132.
(32) Adams, P. D., Afonine, P. V., Bunkoczi, G., Chen, V. B., Davis, I. W., Echols, N., Headd, J. J., Hung, L.-W., Kapral, G. J., Grosse-Kunstleve, R. W., McCoy, A. J., Moriarty, N. W., Oeffner, R., Read, R. J., Richardson, D. C., Richardson, J. S., Terwilliger, T. C., and Zwart, P. H. (2002) PHENIX: A comprehensive Python-based system for macromolecular structure solution. *Acta Crystallogr. D66*, 213−221.
(33) Laskowski, R. A., MacArthur, M. W., Moss, D. S., and Thornton, J. M. (1993) PROCHECK: A program to check the stereochemical quality of protein structures. *J. Appl. Crystallogr. 26*, 283−291.
(34) DeLano, W. L. (2002) *The PyMOL Molecular Graphics System*, DeLano Scientific, San Carlos, CA.
(35) Cole, L. J., Entsch, B., Ortiz-Maldonado, M., and Ballou, D. P. (2005) Properties of *p*-Hydroxybenzoate Hydroxylase When Stabilized in Its Open Conformation. *Biochemistry 44*, 14807−14817.
(36) Holm, L., and Rosenstrom, P. (2010) Dali server: Conservation mapping in 3D. *Nucleic Acids Res. 38*, W545−W549.
(37) Mohanty, S. K., Yu, C.-L., Das, S., Louie, T. M., Gakhar, L., and Subramanian, M. (2012) Delineation of the caffeine C-8 oxidation pathway in *Pseudomonas* sp. strain CBB1 via characterization of a new trimethyluric acid monooxygenase and genes involved in trimethyluric acid metabolism. *J. Bacteriol. 194*, 3872−3882.
(38) Enroth, C., Neujahr, H., Schneider, G., and Lindqvist, Y. (1998) The crystal structure of phenol hydroxylase in complex with FAD and phenol provides evidence for a concerted conformational change in the enzyme and its cofactor during catalysis. *Structure 6*, 605−617.
(39) Hiromoto, T., Fujiwara, S., Hosokawa, K., and Yamaguchi, H. (2006) Crystal Structure of 3-Hydroxybenzoate Hydroxylase from *Comamonas testosteroni* Has a Large Tunnel for Substrate and Oxygen Access to the Active Site. *J. Mol. Biol. 364*, 878−896.
(40) McCulloch, K. M., Mukherjee, T., Begley, T. P., and Ealick, S. E. (2009) Structure of the PLP Degradative Enzyme 2-Methyl-3-hydroxypyridine-5-carboxylic Acid Oxygenase from *Mesorhizobium loti* MAFF303099 and Its Mechanistic Implications. *Biochemistry 48*, 4139−4149.
(41) Treiber, N., and Schulz, G. E. (2008) Structure of 2,6-Dihydroxypyridine 3-hydroxylase from a Nicotine-degrading Pathway. *J. Mol. Biol. 379*, 94−104.
(42) Cole, L. J., Gatti, D. L., Entsch, B., and Ballou, D. P. (2005) Removal of a Methyl Group Causes Global Changes in *p*-Hydroxybenzoate Hydroxylase. *Biochemistry 44*, 8047−8058.
(43) Ryan, K. S., Chakraborty, S., Howard-Jones, A. R., Walsh, C. T., Ballou, D. P., and Drennan, C. L. (2008) The FAD Cofactor of RebC Shifts to an IN Conformation upon Flavin Reduction. *Biochemistry 47*, 13506−13513.
(44) Wang, J., Ortiz-Maldonado, M., Entsch, B., Massey, V., Ballou, D., and Gatti, D. L. (2002) Protein and ligand dynamics in 4-hydroxybenzoate hydroxylase. *Proc. Natl. Acad. Sci. U.S.A. 99*, 608−613.
(45) Entsch, B., and van Berkel, W. J. (1995) Structure and mechanism of para-hydroxybenzoate hydroxylase. *FASEB J. 9*, 476−483.
(46) Retailleau, P., Colloch, N., Vivares, D., Bonnete, F., Castro, B., El Hajji, M., Mornon, J.-P., Monard, G., and Prange, T. (2004) Complexed and ligand-free high-resolution structures of urate oxidase (Uox) from *Aspergillus flavus*: A reassignment of the active-site binding mode. *Acta Crystallogr. D60*, 453−462.